



# Loss of function mutations in *VARS* encoding cytoplasmic valyl-tRNA synthetase cause microcephaly, seizures, and progressive cerebral atrophy

Joshi Stephen<sup>1</sup> · Sheela Nampoothiri<sup>2</sup> · Aditi Banerjee<sup>3</sup> · Nathaniel J. Tolman<sup>4</sup> · Josef Martin Penninger<sup>5</sup> · Ullrich Elling<sup>5</sup> · Chukwuma A. Agu<sup>5</sup> · John D. Burke<sup>1</sup> · Kalpana Devadathan<sup>6</sup> · Rajesh Kannan<sup>7</sup> · Yan Huang<sup>8</sup> · Peter J. Steinbach<sup>9</sup> · Susan A. Martinis<sup>3</sup> · William A. Gahl<sup>1,4,8</sup> · May Christine V. Malicdan<sup>1,4,8</sup>

Received: 12 January 2018 / Accepted: 12 April 2018 / Published online: 24 April 2018  
© Springer-Verlag GmbH Germany, part of Springer Nature 2018 (outside the usa) 2018

## Abstract

Progressive microcephaly and neurodegeneration are genetically heterogeneous conditions, largely associated with genes that are essential for the survival of neurons. In this study, we interrogate the genetic etiology of two siblings from a non-consanguineous family with severe early onset of neurological manifestations. Whole exome sequencing identified novel compound heterozygous mutations in *VARS* that segregated with the proband: a missense (c.3192G>A; p.Met1064Ile) and a splice site mutation (c.1577-2A>G). The *VARS* gene encodes cytoplasmic valyl-tRNA synthetase (ValRS), an enzyme that is essential during eukaryotic translation. cDNA analysis on patient derived fibroblasts revealed that the splice site acceptor variant allele led to nonsense mediated decay, thus resulting in a null allele. Three-dimensional modeling of ValRS predicts that the missense mutation lies in a highly conserved region and could alter side chain packing, thus affecting tRNA binding or destabilizing the interface between the catalytic and tRNA binding domains. Further quantitation of the expression of *VARS* showed remarkably reduced levels of mRNA and protein in skin derived fibroblasts. Aminoacylation experiments on patient derived cells showed markedly reduced enzyme activity of ValRS suggesting the mutations to be loss of function. Bi-allelic mutations in cytoplasmic amino acyl tRNA synthetases are well-known for their role in neurodegenerative disorders, yet human disorders associated with *VARS* mutations have not yet been clinically well characterized. Our study describes the phenotype associated with recessive *VARS* mutations and further functional delineation of the pathogenicity of novel variants identified, which widens the clinical and genetic spectrum of patients with progressive microcephaly.

**Electronic supplementary material** The online version of this article (<https://doi.org/10.1007/s00439-018-1882-3>) contains supplementary material, which is available to authorized users.

✉ May Christine V. Malicdan  
malicdanm@mail.nih.gov

<sup>1</sup> Section of Human Biochemical Genetics, Medical Genetics Branch, National Human Genome Research Institute, National Institutes of Health, Bethesda, MD, USA

<sup>2</sup> Department of Pediatric Genetics, Amrita Institute of Medical Sciences and Research Center, Cochin, Kerala, India

<sup>3</sup> Department of Biochemistry, University of Illinois at Urbana-Champaign, Urbana, IL, USA

<sup>4</sup> Office of the Clinical Director, National Human Genome Research Institute (NHGRI), National Institutes of Health, Bethesda, MD, USA

<sup>5</sup> Institute of Molecular Biotechnology of the Austrian Academy of Science (IMBA), Vienna Biocenter (VBC), Dr. Bohr Gasse 3, Vienna, Austria

<sup>6</sup> Department of Pediatric Neurology, KIMS Hospital, Thiruvananthapuram, Kerala, India

<sup>7</sup> Department of Radiology, Amrita Institute of Medical Sciences and Research Center, Cochin, Kerala, India

<sup>8</sup> NIH Undiagnosed Diseases Program, National Human Genome Research Institute (NHGRI) and the Common Fund, National Institutes of Health, Bethesda, MD, USA

<sup>9</sup> Center for Molecular Modeling, Center for Information Technology, National Institutes of Health, Bethesda, MD, USA

## Introduction

Microcephaly is a genetically heterogeneous neurodevelopmental disorder characterized by marked reduction in brain size accompanied by varying degrees of intellectual disability, seizures and abnormal facial features that manifest either congenitally or progressively within 1 or 2 years of birth. Major cases of congenital primary microcephaly are due to defects in genes involved in transcription regulation, cell cycle progression, centrosome maturation, mitotic spindle formation, and migration of neuronal cells (Barkovich et al. 2012). In contrast to congenital microcephaly, progressive or post-migrational microcephaly is commonly accompanied by cerebral–cerebellar atrophy and associated neurodegenerative diseases. Mutations in genes involved in transcription and translation machinery largely account for the latter condition, one of which includes the amino acyl-tRNA synthetases (ARSs) family of genes (Antonellis and Green 2008). ARSs comprise an ancient group of housekeeping enzymes catalyzing the esterification of amino acids with their cognate tRNA bearing correct anticodon, to translate information to the protein level with high fidelity (Havrylenko and Mirande 2015). In human cells, there are 37 different ARSs encoded by different genes, 18 of which function exclusively in the cytoplasm, and 17 in the mitochondria, and the remaining two in both cell compartments. Mitochondrial ARS are implicated in autosomal recessive diseases affecting multiple organs, while genes encoding cytoplasmic ARS are generally inherited in both dominant and recessive fashion. Dominant mutations in cytoplasmic ARSs (cARSs) cause peripheral neuropathies such as Charcot Marie Tooth (CMT) diseases (Oprescu et al. 2017) and muscular dystrophy (Tsai et al. 2017). Most of the recessive cARSs mutations (*AARS*, *DARS*, *IARS*, *LARS*, *RARS*, *SARS*) are associated with severe neurological manifestations including epileptic encephalopathy, hypo myelination, microcephaly, neurodegeneration, growth retardation, and intellectual disability (Kopajtich et al. 2016; Latour et al. 2010; Musante et al. 2017; Taft et al. 2013; Wolf et al. 2014; Zhang et al. 2014). However, interstitial lung and liver diseases in *LARS*, *MARS*, and Usher syndrome type 3B in *HARS* have also been identified, suggesting diverse functions of individual ARSs (Casey et al. 2012; Gonzalez et al. 2013).

Here we describe two siblings presented with progressive microcephaly, brain atrophy and seizures. Through whole exome sequencing (WES), we identified bi-allelic mutations in *VARS*, encoding the cytoplasmic valyl-tRNA synthetase (ValRS) as the probable causative variants.

## Materials and methods

### Study subjects

Patients were clinically evaluated at the Amrita Institute of Medical Sciences, Kerala, India. Written informed consent for clinical details, photography and sample collection was obtained from parents under the protocol 76-HG-0238 (Diagnosis and treatment of patients with inborn errors of metabolism or other genetic disorders) approved by the Institutional Review Board of the National Human Genome Research Institute.

### Whole exome sequencing

Whole exome sequencing was performed using the Agilent Sure Select Target Enrichment Kit and the Illumina HiSeq 2000/2500 sequencer (Illumina, San Diego, CA) according to manufacturer's instructions. Identified reads were aligned to a human reference genome (hg19; NCBI build 37; Feb. 2009), variant calling files were generated (Genome Analysis Tool Kit, Broad Institute) and functionally annotated using ANNOVAR (Chang and Wang 2012). Variants were filtered based on allele frequency less than 0.01 with truncating nature of the variants and predicted pathogenicity according to an online prediction tool (Supplementary Table 1). Identified candidates were Sanger evaluated for confirmation and family segregation. The novel variants identified in this study have been deposited in the Leiden Open Variation Database (LOVD) and now publicly available online (<https://databases.lovd.nl/share/d/transcripts/00022556>).

### Cell culture

Patient fibroblasts were cultured from skin biopsy as described (Stephen et al. 2016). Human normal fibroblast cell lines purchased from ATCC (Manassas, VA, USA) and Coriell (Camden, NJ, USA) were used as controls for our experiments. Fibroblasts were cultured and maintained in high-glucose (4.5 g/L) DMEM with 10% fetal bovine serum (FBS; Gemini Bio-Products, West Sacramento, CA, USA), 1% MEM non-essential amino acid solution and 1% penicillin–streptomycin with glutamine. Mouse embryonic haploid stem cells were generated as previously described (Elling et al. 2011, 2017) and transferred to feeder-free conditions using Matrigel (BD Biosciences) and maintained with standard mouse embryonic cell culture media (Sigma). Both human and mouse cell lines were lysed using RIPA buffer (Sigma) and quantified as described previously (Stephen et al. 2017). *VARS* native overexpression lysate was

purchased from Novus Biologicals (NBP2-07645) and used for western blotting.

### Splicing analysis

Total RNA was extracted from the patient skin derived fibroblasts using the RNeasy Mini Kit (Qiagen, CA, USA). cDNA synthesis was performed using a High Capacity RNA to cDNA synthesis kit (Applied Biosystems) according to the manufacturer's protocol. Primers specific to two predominant transcripts were designed (Supplementary Table 2), amplified by PCR and further evaluated by Sanger sequencing.

### Quantitative RT-PCR and western blotting

Relative mRNA expression level of *VARS* was measured in patient skin fibroblasts using SYBR Green PCR master mix and analyzed as described elsewhere (Stephen et al. 2016). Primers probes used for qPCR are shown in supplementary Table 2. For western blotting, protein lysates derived from fibroblasts were electrophoresed on 3–8% Tris-Acetate gel, blotted on nitrocellulose membrane and treated with the primary Anti-VARS monoclonal antibody produced in rabbit that targets the N-terminal region of VARS (Abcam). Immunoblots were treated with appropriate secondary antibodies and imaged under IR Odyssey® Imaging System (LiCOR, Lincoln, NE).

### Homology modeling

The crystal structure of a complex of *Thermus thermophilus* valyl-tRNA synthetase (ValRS) and tRNA<sup>Val</sup> (pdb code: 1gax) (Fukai et al. 2000) was used as the template to build a three-dimensional model of the human ValRS complex. The Prime software tools (Schrodinger, LLC) were used to build the model, which was subsequently refined to relieve strain in and around Phe 1063. Using CHARMM (Brooks et al. 2009), the phenylalanine side chain was rebuilt with ideal geometry, and the energy calculated with the SCPISM solvent description (Hassan and Steinbach 2011) was minimized while allowing only residues Cys 927, Phe 1007, Thr 1011, and Phe 1063 to move. The model was rendered using the programs MolScript (Kraulis 1991) and Raster3D (Merritt and Bacon 1997).

### Aminoacylation assay

Bovine liver crude tRNA (Sigma) was re-suspended in 1 mL of 10 mM HEPES pH 7.5, 0.1 mM EDTA. Since mammalian tRNA often lacks CCA at the 3'-end, a previously published method was employed to process the tRNA using *E. coli* CCA-adding enzyme, with the exception of utilizing a

temperature of 37 °C (Pang and Martinis 2009). The full-length tRNA was phenol-extracted using 2 mL Phase Lock Gel tubes (Eppendorf) and subsequently ethanol-precipitated overnight. The tRNA was re-suspended in 10 mM HEPES buffer pH 7.5, 0.1 mM EDTA for use in aminoacylation reaction. Aminoacylation was carried out in the presence of 50 mM HEPES, pH 7.4, 15 mM MgCl<sub>2</sub>, 20 mM KCl, 1 mM dithiothreitol, 50 μM L-[<sup>14</sup>C]-valine (0.27 Ci/mmol), 1.5 mg/mL of full length bovine liver tRNA and mouse embryonic cell lysate containing 320 μg/mL of protein or human fibroblast cell lysate at 920 μg/mL. The human fibroblast lysate had reduced expression of ValRS when compared to the mouse embryonic stem cell lysates. Therefore, to carry out the aminoacylation assay, the lysates from human fibroblast cells were used at a higher protein concentration with equal overall protein concentration. Aliquots (5 μL) were taken at different time points and quenched on Whatman filter pads that were pre-soaked with 10% trichloroacetic acid (TCA). The pads were washed three times for 8 min each with ice-cold 5% TCA and then treated with ice-cold 95% ethanol for 8 min. The washed pads were then dried under a heat lamp. Radioactivity was quantified in a Beckman LS 6500 scintillation counter (Beckman Coulter, Fullerton, CA).

## Results

### Clinical features

The elder sibling of the proband (Fig. 1a-II.1) was born at 32 weeks of gestation, had a birth weight of 2160 g (50th–75th centile), birth length of 40 cm (<5th centile) and head circumference of 28 cm (<3rd centile, –6SD); his mother had gestational diabetes during the pregnancy and was on diet control. The infant had a very small anterior fontanel and prominent sutural ridging and weak cry. He had progressive microcephaly and developed seizures by the first month of age (Fig. 1b). The head circumference at 2 months was only 30 cm (<3rd centile, –8SD). He did not acquire any motor milestones or speech and expired at 1 year of age due to a severe respiratory infection. He had an episode of status epilepticus by 30 days of life and had recurrent lower respiratory tract infections. There was no record of hepatosplenomegaly. The metabolic evaluation did not reveal any abnormality. Brain stem auditory evoked response showed bilateral conductive hearing loss. Ophthalmological evaluation showed a myopic astigmatism of 3D and visual evoked response revealed prolonged P100 latency. Plain CT of the brain in the new-born appeared normal and there was no intracranial calcification. Axial T2 and coronal T2 MRI of brain at 4 months of age showed diffuse cerebral atrophy with thinning of corpus callosum and normal cerebellum (Fig. 1c, d). There was no diffusion restriction.

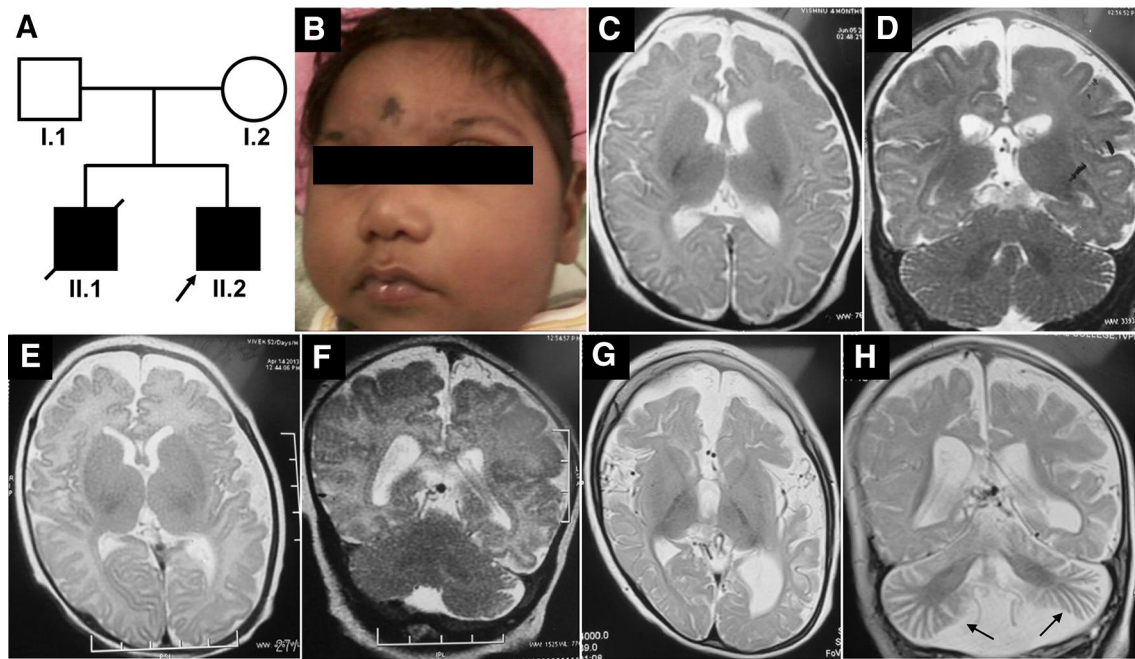


**Fig. 1** Pedigree and clinical features of the family. **a** Pedigree of the family (arrow points to the proband). **b** Clinical photographs of the elder sibling of the proband (A-II.1) showing severe microcephaly, low set ears, upslant of eyes, sloping forehead, micrognathia, short nose and flat nasal bridge. **c, d** MRI of A-II.1 at the age of 4 months showing diffuse cerebral atrophy, thin corpus callosum and normal

cerebellum. **e, f** T2 Axial and coronal MRI images of the proband (A-II.2) at 52 days of life showing minimal diffuse brain atrophy with prominent fissures and sulci and no significant cerebellar atrophy. **g, h** MRI repeated at 2 years of proband (A-II.2) showing progressive worsening of cerebral and cerebellar atrophy (arrow in H) and thinning of corpus callosum

The Proband (Fig. 1a-II.2) was a 32-month-old male born as the second child of a non-consanguineous couple from India, evaluated for global developmental delay. He was born as a full-term baby following caesarean section due to breech presentation. His mother (Fig. 1a-I.2) had gestational diabetes in the second pregnancy and was managed with insulin. At birth, he had a birth weight of 4070 g (75th–90th centile) and a head circumference of 33 cm (10th centile, – 2SD). At around 1.4 months of age (49 days) he had right focal seizures, of no obvious etiology, but was diagnosed to have anemia, which was corrected with a single blood transfusion. At 2 months, his head circumference was noticeable smaller for age (34.5 cm, < 3rd centile, – 4SD). During the most recent hospital visit at 32 months, he continued to have refractory seizures that were moderately controlled by five antiepileptic medications. On examination, he had severe microcephaly (40 cm, < 3rd centile, between – 8SD and – 9SD), bilaterally low set ears, long eyelashes, sloping forehead, micrognathia, and short nose. He did not attain head control and speech. He had generalized hypotonia; deep tendon reflexes were present in the upper extremity but were not elicited at the knees and ankles. He also had contracture of ankles and clawing of fingers. Because he had difficulty in swallowing, he was fed through a nasogastric tube. Axial T2 plain sequences of magnetic resonance

imaging (MRI) of brain done at 52 days of life showed minimal diffuse brain atrophy with prominent fissures and sulci (Fig. 1e). Coronal T2 imaging did not show significant cerebellar atrophy (Fig. 1f). MRI brain imaging repeated at 2 years of life showed progressive worsening of cerebral and cerebellar atrophy, reduction in white matter volume, bilateral frontal and occipital subcortical white matter hyperintensities and thinning of corpus callosum in Axial T2 coronal T2 sequences (Fig. 1g, h). Unusually prominent vascular flow voids were noted along cerebrospinal fluid spaces especially over temporal polar and over convexities in coronal T2 sequence. Electroencephalogram showed bilateral occipital epileptiform abnormalities. Fundus evaluation was normal. Echocardiogram, visual evoked potential, TORCH screening, and immunoglobulin estimation in serum were normal. Flow cytometry revealed a normal level of CD3 and CD19 (CD3–65.8%, CD19–17.9%). A comprehensive clinical summary of both the patients is shown in Table 1.

Karyotype analysis of the proband (II.2) showed 46 XY. Metabolic screening with tandem mass spectrometry and gas chromatography of urine sample did not suggest an underlying metabolic defect. A stress cytogenetics study using mitomycin C showed increased chromosomal breakages. In view of microcephaly, sloping forehead, diffuse

**Table 1** Clinical summary of the patients

Clinical features	I-II.1	I-II.2
Ethnicity	Indian (Asian)	Indian (Asian)
Consanguinity	No	No
Mutations identified in <i>VARS</i> (Ref. NM_006295.2)	NA	Chr6:31752087T>C: c.1577-2A>G;p.? and Chr6:31747481C>T: c.3192G>A;p.M1064I
Age	Expired at 1 year of age	3 years of age
Gender	Male	Male
Growth		
Birth weight	2160 g (50th–75th centile)	4070 g (75th–90th centile)
Birth length	40 cm (<5th centile)	NA
Birth head circumference	28 cm (<3rd centile, -6SD)	33 cm (10th centile, - 2SD)
Recent height	NA	NA
Recent weight	NA	NA
Recent head circumference	30 cm (<3rd centile, - 8SD) at 2 months	40 cm (<3rd centile, between - 8SD to - 9SD)
Neurologic features		
Motor developmental delay	Yes	Yes
Thin corpus callosum	Yes	Yes
Seizures	Yes	Yes
EEG	NA	Bilateral occipital abnormalities
Speech delay	Yes	Yes
Microcephaly	Yes	Yes
MRI	Cerebral atrophy and normal cerebellum	Progressive cerebral and cerebellar atrophy, reduction in white matter volume
Hearing	Hearing loss	NA
Facial features	Low set ears, upslant of eyes, micrognathia, short nose, flat nasal bridge	Low set ears, long eye lashes, sloping forehead, short nose, micrognathia
Ophthalmological features	Myopic astigmatism	Normal fundus
Muscle tone	NA	Hypotonia, deep tendon reflexes
Cardiac abnormalities	NA	Normal ECG
Skeletal features	NA	Normal
Respiratory features	Infection	Normal
Immunological features	Recurrent respiratory tract infection	TORCH screening and serum Ig normal, CD3 and CD19 normal
Gastrointestinal features	NA	Swallowing difficulties so fed through nasogastric tube
Genitourinary features	NA	NA
Other features	Very small anterior fontanel, weak cry	No head control, swallowing difficulty, vascular flow voids in cerebrospinal fluid spaces

NA not available

brain atrophy and increased chromosomal breakages, and a family history a microcephaly and death in a sibling, the possibility of Nijmegen breakage syndrome was considered but no mutations in *NBN* were found. Clinical exome sequencing of a panel of genes (4829 genes), including known disease-causing genes of microcephaly, did not identify any pathogenic mutations. Hence, trio WES (parents and the proband) was performed to identify the underlying genetic cause. DNA samples from the elder sibling of the proband (II.1) were unavailable for the clinical genetic evaluation.

### Identification of mutations in *VARS*, splice analysis and protein modeling

Exome sequencing followed by variant filtering identified compound heterozygous mutations in *VARS*: a splice site mutation, Chr6:31752087T>C (NM\_006295.2:c.1577-2A>G;p.?) inherited from father and a missense mutation, Chr6:31747481C>T (NM\_006295.2:c.3192G>A;p.Met1064Ile) inherited from mother (Fig. 2a). A summary of exome analysis and the final list of variants are given in supplementary Table 1. Both the mutations in *VARS* are novel (not found in any online databases

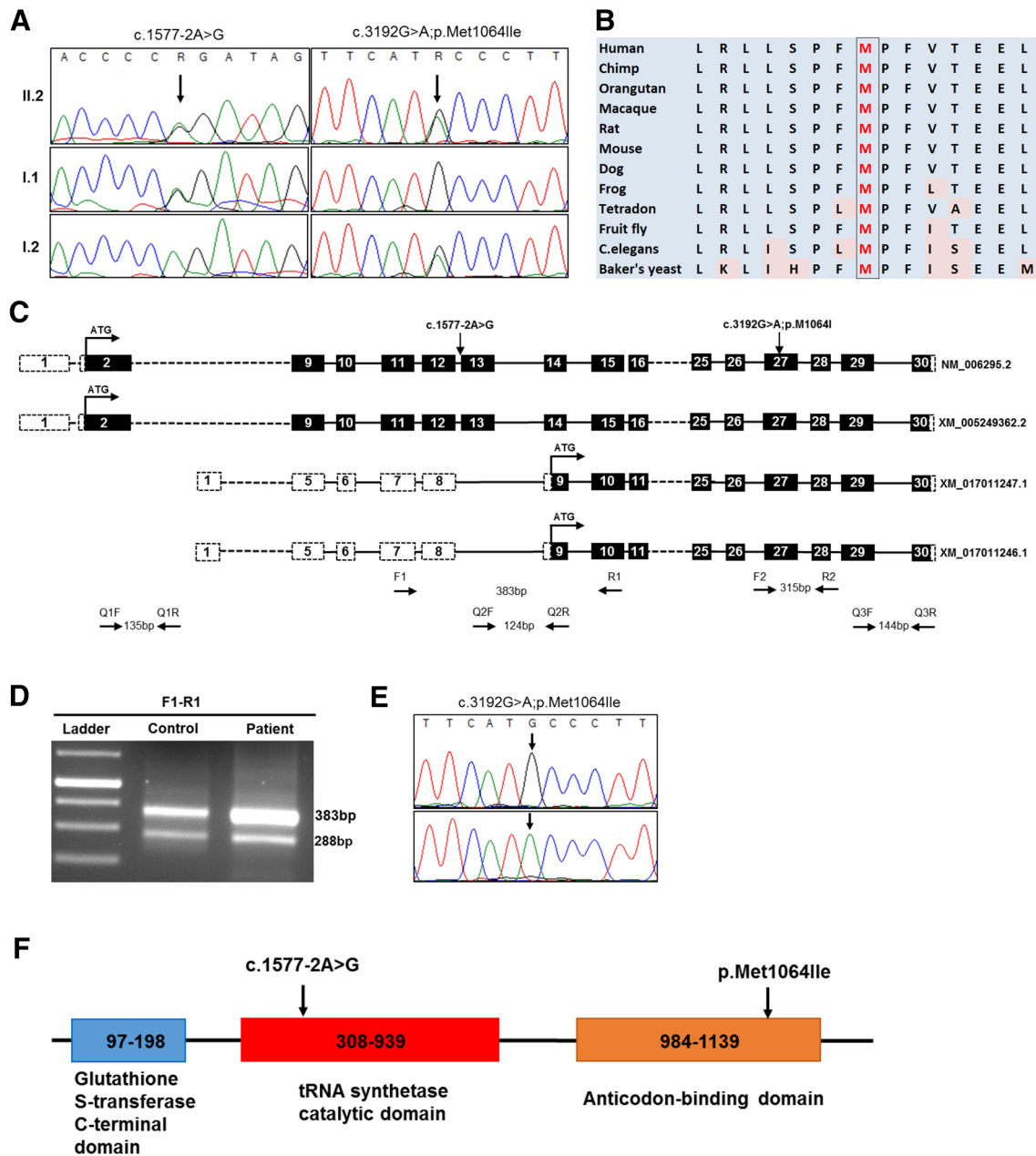


**Fig. 2** Sanger validation of the variants, conservation and splice analysis. **a** Sanger validation of identified compound heterozygous variants in the proband: the splice site variation (c.1577-2A>G) inherited from the father and the missense variation (c.3192G>A) inherited from the mother. **b** Conservation of amino acids around the position of missense variation (c.3192G>A; p.Met1064Ile); methionine is highly conserved up to *C.elegans* and *Baker's yeast*. **c** Diagrammatic representation of different splice variants of *VARS* and primer designing scheme for splice analysis and qPCR. Each box represents the exonic regions of the gene; the black boxes are coding parts and the boxes with dashed line denote untranslated regions, and 'ATG' marks the start of the coding frame. Two splice variants (XM\_017011247.1 and XM\_017011246.1) lack 5' coding regions and exon 13 compared to the longest variants (NM\_006295.2 and XM\_005249362.2) and have their start codon in-frame downstream. Position of prim-

ers for splice defect analysis (F1–R1, F2–R2) and qPCR (Q1F–Q1R, Q2F–Q2R, Q3F–Q3R) are also depicted. **d** Gel images of the PCR products of F1–R1 flanking the splice site mutation. The lower band (288 bp) which lacks exon 13 is present in both control and patient, results from the amplification of shorter splice variants that lack exon 13. **e** Chromatogram showing the sequencing results of F2–R2 amplifying cDNA, depicting the presence of only one allele (c.3192A) in the patient (lower panel) compared to control (upper panel), showing the absence of G allele, which harbors the splice site variation. **f** Schematic representation of different functional domains in the full length *VARS* protein (Uniprot: P26640). The splice site variation is predicted to abolish both tRNA synthetase and anticodon-binding domains while the missense variation is in a highly conserved area of the anticodon-binding domain

ExAC, genomAD) and have high CADD Phred scores (17.55 and 23.7, respectively). The missense mutation is predicted to be damaging per various prediction tools: SIFT (score: 0), Mutation Taster ( $p$  value: 1), and PolyPhen-2 (score: 0.99), and located in the highly conserved area of the anticodon-binding domain of the protein (Fig. 2b). The splice site mutation is in the canonical acceptor splice site before exon 13 which encodes a part of the catalytic domain of the enzyme. Exon 13 resides in the intronic region of two predicted splice variants, XM\_017011246.1 and XM\_017011247.1 (Fig. 2c). Both control and patient's cDNA amplification showed two bands: the upper band (383 bp) for the longest isoform; and the lower one (288 bp), which naturally lacks exon 13, for the other two isoforms (Fig. 2d). Skipping of exon 13 is predicted to lead to premature termination codon (NM\_006295.2:c.1577\_1671del; p.(Asp526Alafs\*22) and result in the degradation of mutant mRNA through nonsense mediated decay. This was supported by the finding that amplification of the missense mutation at exon 27 on concentrated cDNA showed a single mutant peak (c.3192A) in the patient compared to the control, which indicates that the mRNA allele harboring the splice site variation is severely reduced or absent (Fig. 2e). Thus, both the missense and splice site mutations are predicted to affect the functional domains of the ValRS suggesting the possible pathogenicity (Fig. 2f).

To assess the possible functional impact of the missense mutation (M1064I), a model of human ValRS bound to tRNA was generated using the template crystal structure of *Thermus thermophilus* valyl-tRNA synthetase (ValRS) and tRNA<sup>Val</sup> complex (Fig. 3a). The highly conserved region surrounding Met 1064 (position of missense variation) is shown in Fig. 3b. Note that although Cys 950 corresponds to an alanine in the *Thermus thermophilus* template structure, cysteine is, in fact, highly conserved at this position (alignment not shown). Thus, the neighboring residues of Met 1064 are highly conserved, and the mutation M1064I presumably alters side chain packing, possibly displacing the nearby alpha helix that includes Cys 950 and conserved residues that are proximal to the bound tRNA, namely, Arg947, Asn951, Lys952, Asn955, Ala956, and Phe959 (Fig. 3c). The mutation may also destabilize the interface between the catalytic domain and the anticodon-binding domain. In the Conserved Domain Database (Marchler-Bauer et al. 2017), residues 335–938, including the conserved DALR motif, are assigned to the catalytic core domain, and the anticodon-binding domain ranges from residue 938–1075. It is possible that the M1064I variant perturbs the association of these domains, straining the ValRS structure and possibly shifting residues near the aminoacylation site, which could affect the amino acylation activity of the enzyme (Fig. 3c).

## Expression of VARS is severely reduced in patient skin fibroblasts

Valyl-tRNA synthetase is ubiquitously expressed in tissues, including skin, with a diverse array of cellular functions (Lo et al. 2014). We measured the level of mRNA in skin derived fibroblasts from the patient using three different primer probes specific to the N-terminal (Q1F–Q1R), middle (Q2F–Q2R) and C-terminal (Q3F–Q3R) regions of the transcripts (Fig. 2c). Supplementary Table 2 lists the sequence information for each primer probes. Realtime PCR amplification using the three primer probes showed significant reduction of transcripts (50–60%) in patient compared to control (Fig. 4a). Further examination of protein expression levels using immunoblotting showed severely reduced expression of VARS protein in the proband cells (Fig. 4b). Note that in control cell lines, there is some degree of variability in protein expression.

## Aminoacylation is reduced in patient derived fibroblasts

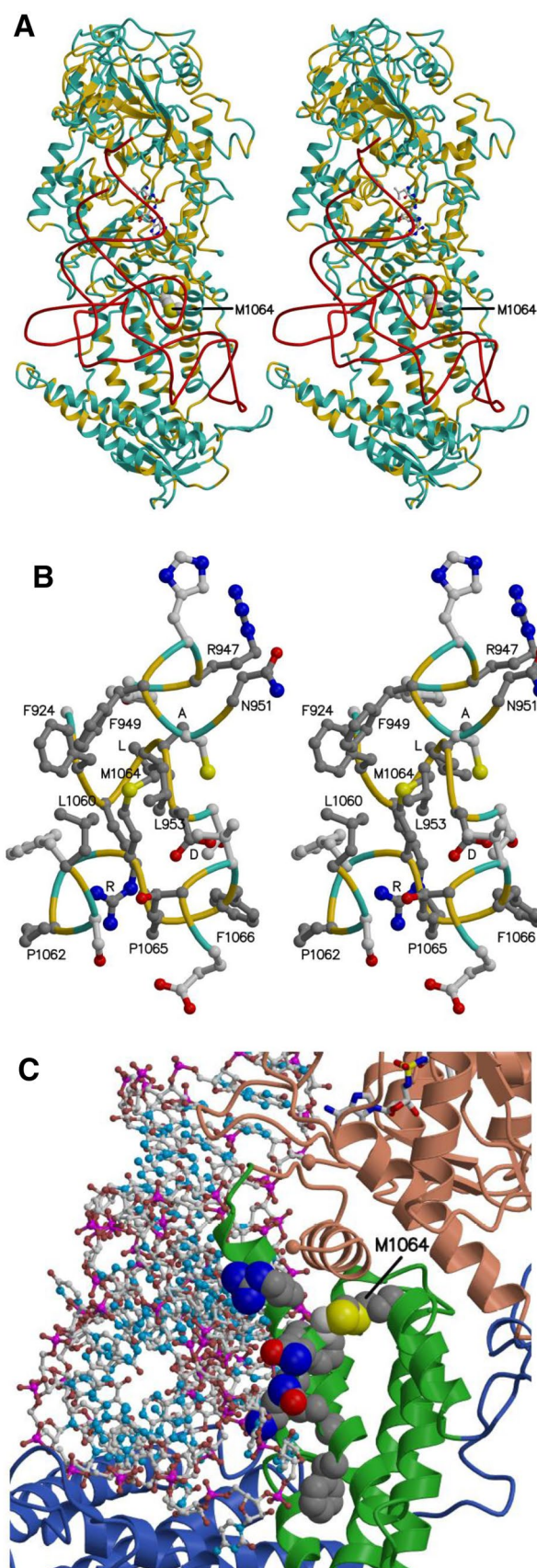
ValRS recognizes tRNA<sup>Val</sup> via the C-terminal anticodon-binding domain's interactions with A<sub>35</sub> and C<sub>36</sub> anticodon identity elements of tRNA<sup>Val</sup> (Tamura et al. 1991). X-ray crystallographic studies on *T. thermophilus* ValRS have confirmed these interactions (Fukai et al. 2003). Nucleotides A<sub>35</sub> and C<sub>36</sub> form base stacking interactions with a conserved Phe residue from the anticodon-binding domain of ValRS. The first and third helices of this domain of ValRS contact the tRNA<sup>Val</sup> and help hold it in position. Sequence alignment shows that Met1064 is a conserved residue of the anticodon-binding domain (Fig. 2b, f). Though this residue is not directly involved in the interaction between ValRS and tRNA<sup>Val</sup>, it is located near the turn of the second helix of the anticodon-binding domain. Mutation of this residue possibly results in structural changes that influence the activity of ValRS, and the other allele with the splice mutation is predicted to be null due to the splice defect. Aminoacylation activity of lysates from patient fibroblast cells was tested in the presence of bovine total tRNA. Compared to three different biological control fibroblast cells, lysate from the patient had about four times reduced aminoacylation activity of ValRS (Fig. 4c) which could possibly impact protein synthesis and affect cellular metabolism. Embryonic stem cells derived from wild type (*Vars*<sup>+/+</sup>) and knock out (*Vars*<sup>-/-</sup>) mice were used as experimental controls to optimize the aminoacylation experiment (Fig. 4D).

**Fig. 3** The model of human valyl-tRNA synthetase with tRNA bound. **a, b** The protein main chain (alpha-carbon atoms) is colored according to sequence identity with the template structure, yellow where identical (39%) and light blue where different. **a** Stereo view, with the tRNA backbone (phosphorus atoms) shown in red, a Val-AMP analog shown as ball and stick, bound in the aminoacylation site, and the side chain of Met 1064 shown as space filling. The location of an unmodeled region inserted in the human sequence between the KMSKS loop and the DALR motif is marked by the blue spheres representing Asp 875 and Cys 917. **b** Stereo view of residues neighboring Met 1064, with carbon atoms in side chains of residues identical in the model and template colored dark gray. The DALR motif and other conserved residues are labeled. For clarity, only the tip of Leu 953 is shown. **c** Protein-tRNA interface, with tRNA shown as ball and stick and the Val-AMP analogue shown as sticks. The possible impact of the M1064I mutation on ValRS-tRNA binding is illustrated by showing side chains as space filling for Met 1064 and Cys 950, as well as for conserved residues at or near the interface: Arg 947, Phe 949, Asn 951, Lys 952, Asn 955, Ala 956, and Phe 959. The M1064I mutation might also perturb the interface between the catalytic core domain (colored salmon) and the anticodon-binding domain (green)

## Discussion

The human brain is particularly sensitive to defects in genes involved in transcriptional, RNA processing and translational machinery. Bi-allelic loss of function mutations in genes encoding cytoplasmic aminoacyl tRNA synthetase are implicated for overlapping neurological abnormalities, peripheral neuropathy, liver dysfunction, lung fibrosis, visual and hearing impairment; for instance, mutations in *AARS*, *RARS*, *DARS*, and *QARS* account for core neurological manifestations including cerebral atrophy, seizures, hypo myelination and microcephaly (Supplementary Table 3). This study reports a family with recessive mutations in *VARS* causing such severe early onset neurological manifestations. The elder sibling of the proband (II.1) manifested severe phenotype and expired at 1 year of age. DNA samples from him were unavailable for analysis. However, similar clinical presentation compared to proband suggests that he probably harbored the same mutations.

Exome sequencing followed by variant filtering revealed bi-allelic variants in five candidate genes: *HTRA4*, *LEXM*, *TLDC2*, *SPEM2*, and *VARS*. *HTRA4* is mainly expressed in placenta and is associated with endothelial dysfunction and capillary leakage (Singh et al. 2015). The *TLDC2* gene has not yet been explored for any specific cellular function. In addition, healthy homozygotes have been reported for at least one of the variants of both *HTRA4* and *TLDC2*, so we excluded them. Among the final three candidates (Supplementary Table 1), *LEXM* encodes an expansion molecule that may have a role in T-cell proliferation. *SPEM2* is highly expressed in testes and knockout models have an abnormal reproductive system; so its role appears to be in reproduction. On the other hand, variants in the *VARS* gene had a comparatively higher CADD score (Supplementary Table 1)





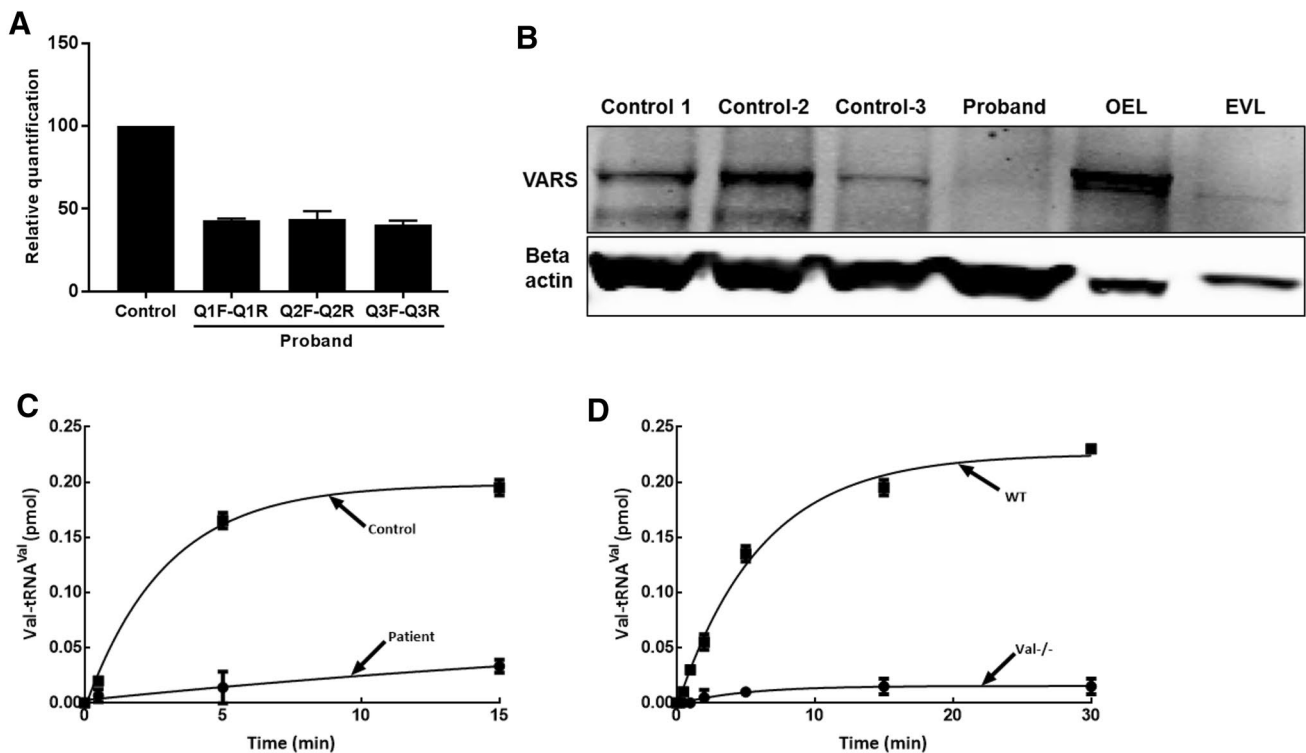


**Fig. 4** VARS expression studies and aminoacylation activity in proband cells. **a** VARS mRNA expression studies using three different primer probes (see the primer designing scheme in Fig. 2c) showing 50–60% reduction of transcripts in proband, relative to control. **b** VARS immunoblotting using cell lysates derived from three controls and proband showing severe reduction in protein expression in proband cells. VARS overexpression lysate (OEL) produced in HEK293T cells was used as positive control and compared to empty vector lysate (EVL) (Novus Biologicals, NBP2-07645). Results were normalized to beta actin loading control. **c, d** Decreased aminoacyla-

tion activity in proband fibroblast cell lysate. Valylation was carried out using cell lysate containing 920  $\mu\text{g}/\text{mL}$  of protein and 1.5  $\text{mg}/\text{mL}$  full length bovine liver tRNA. **c** Enzyme activity of fibroblasts from control unaffected individual (closed squares) and proband II.2 (closed circles) was measured and normalized with total protein content. Mean values from three different control cell lines are shown. **d** The assay was optimized using mouse embryonic stem cells (wild type, closed squares; knockout, closed circles). All assays were done in triplicates and the error bars represent standard error of means

among our candidates, and the variants are predicted to affect important domains of the protein. Recently, in a large cohort of individuals with neurological malformations, Karaca et al. reported three affected individuals from two unrelated consanguineous families having homozygous missense mutations in *VARS* (Karaca et al. 2015); the affected individuals in the report had phenotypic overlap with our patients, presenting with severe microcephaly, developmental delay, intellectual disability and cortical atrophy. Considering the phenotype similarity and association of other cytoplasmic amino acyl tRNA synthetases (e.g., microcephaly and brain atrophy in patients with mutations in *AARS*, *DARS*, or *QARS*), we chose *VARS* as the best candidate.

ValRS belongs to the class I family of AARs and has high sequence similarity with mitochondrial ValRS, encoded by *VARS2*, the gene recently implicated for encephalomyopathies (Diodato et al. 2014). Like other ARSs, ValRS contains the catalytic domain and the anticodon-binding domain to catalyze the amino acylation of

specific tRNAs; the catalytic domain catalyzes the binding of amino acid and ATP to form aminoacyl intermediate with the release of a pyrophosphate molecule. In a second step, the enzyme recognizes the appropriate tRNA with its anticodon-binding domain and covalently links the tRNA to amino acid to form amino acyl tRNA molecule (Datt and Sharma 2014). The truncating mutation in our patient is predicted to abolish both the catalytic domain and tRNA binding domain, while the missense mutation is in a highly conserved region of the tRNA binding domain (Fig. 2f), potentially affecting both the steps of enzymatic reaction. As per our protein modeling studies, it is possible that the Met1064Ile variant perturbs the association of these domains, straining the ValRS structure and possibly shifting residues near the aminoacylation site. In our mRNA expression studies, we observed 50–60% reduction in the transcripts due to nonsense mediated decay of the allele carrying splice site mutation. However, we observed severe reduction in protein levels, in contrast to mRNA

expression, which could possibly be due to a decreased protein stability of the protein with the missense mutation. The severe defect in aminoacylation we observed in our patient cells correlates with our expression and modeling data. Although the ValRS in-frame splice variants lack a catalytic domain, which has diverse cellular functions (Lo et al. 2014), we did not observe any defect other than neurological problems in our patients.

In conclusion, our study highlights the clinical characterization of individuals with bi-allelic mutations in *VARS* which encode an evolutionarily conserved enzyme essential for eukaryotic translation. *VARS* mutations produce severe neurological implications, illustrating the essential nature of this gene in the development and proper functioning of the nervous system. This study expands the molecular and clinical phenotyping of patients with bi-allelic *VARS* mutations. Mutations in *VARS* should be considered in patients with severe, early onset progressive microcephaly.

**Acknowledgements** We thank patient and family for participating in this study.

**Funding** This work was supported by the Intramural Research Programs of the National Human Genome Research Institute and the Center for Information Technology, National Institutes of Health, USA.

## Compliance with ethical standards

**Conflict of interest** The authors declare that they have no competing interests.

## References

- Antonellis A, Green ED (2008) The role of aminoacyl-tRNA synthetases in genetic diseases. *Annu Rev Genom Hum Genet* 9:87–107. <https://doi.org/10.1146/annurev.genom.9.081307.164204>
- Barkovich AJ, Guerrini R, Kuzniecky RI, Jackson GD, Dobyns WB (2012) A developmental and genetic classification for malformations of cortical development: update 2012. *Brain* 135:1348–1369. <https://doi.org/10.1093/brain/aws019>
- Brooks BR, Brooks CL 3rd, Mackerell AD Jr, Nilsson L, Petrella RJ, Roux B, Won Y, Archontis G, Bartels C, Boresch S, Cafilisch A, Caves L, Cui Q, Dinner AR, Feig M, Fischer S, Gao J, Hodoscek M, Im W, Kuczera K, Lazaridis T, Ma J, Ovchinnikov V, Paci E, Pastor RW, Post CB, Pu JZ, Schaefer M, Tidor B, Venable RM, Woodcock HL, Wu X, Yang W, York DM, Karplus M (2009) CHARMM: the biomolecular simulation program. *J Comput Chem* 30:1545–1614. <https://doi.org/10.1002/jcc.21287>
- Casey JP, McGettigan P, Lynam-Lennon N, McDermott M, Regan R, Conroy J, Bourke B, O’Sullivan J, Crushell E, Lynch S, Ennis S (2012) Identification of a mutation in *LARS* as a novel cause of infantile hepatopathy. *Mol Genet Metab* 106:351–358. <https://doi.org/10.1016/j.ymgme.2012.04.017>
- Chang X, Wang K (2012) wANNOVAR: annotating genetic variants for personal genomes via the web. *J Med Genet* 49:433–436. <https://doi.org/10.1136/jmedgenet-2012-100918>
- Datt M, Sharma A (2014) Evolutionary and structural annotation of disease-associated mutations in human aminoacyl-tRNA synthetases. *BMC Genom* 15:1063. <https://doi.org/10.1186/1471-2164-15-1063>
- Diodato D, Melchionda L, Haack TB, Dallabona C, Baruffini E, Donnini C, Granata T, Ragona F, Balestri P, Margollicci M, Lamantea E, Nasca A, Powell CA, Minczuk M, Strom TM, Meitinger T, Prokisch H, Lamperti C, Zeviani M, Ghezzi D (2014) *VARS2* and *TARS2* mutations in patients with mitochondrial encephalomyopathies. *Hum Mutat* 35:983–989. <https://doi.org/10.1002/humu.22590>
- Elling U, Taubenschmid J, Wirnsberger G, O’Malley R, Demers SP, Vanhaelen Q, Shukalyuk AI, Schmauss G, Schramek D, Schnuetgen F, von Melchner H, Ecker JR, Stanford WL, Zuber J, Stark A, Penninger JM (2011) Forward and reverse genetics through derivation of haploid mouse embryonic stem cells. *Cell Stem Cell* 9:563–574. <https://doi.org/10.1016/j.stem.2011.10.012>
- Elling U, Wimmer RA, Leibbrandt A, Burkard T, Michlits G, Leopoldi A, Micheler T, Abdeen D, Zhuk S, Aspalter IM, Handl C, Liebergesell J, Hubmann M, Husa AM, Kinzer M, Schuller N, Wetzel E, van de Loo N, Martinez JAZ, Estoppey D, Riedl R, Yang F, Fu B, Dechat T, Ivics Z, Agu CA, Bell O, Blaas D, Gerhardt H, Hoepfner D, Stark A, Penninger JM (2017) A reversible haploid mouse embryonic stem cell biobank resource for functional genomics. *Nature* 550:114–118. <https://doi.org/10.1038/nature24027>
- Fukai S, Nureki O, Sekine S, Shimada A, Tao J, Vassilyev DG, Yokoyama S (2000) Structural basis for double-sieve discrimination of L-valine from L-isoleucine and L-threonine by the complex of tRNA(Val) and valyl-tRNA synthetase. *Cell* 103:793–803
- Fukai S, Nureki O, Sekine S-I, Shimada A, Vassilyev DG, Yokoyama S (2003) Mechanism of molecular interactions for tRNA-Val recognition by valyl-tRNA synthetase. *RNA* 9:100–111. <https://doi.org/10.1261/rna.2760703>
- Gonzalez M, McLaughlin H, Houlden H, Guo M, Yo-Tsen L, Hadjivassiliou M, Spezziani F, Yang XL, Antonellis A, Reilly MM, Zuchner S (2013) Exome sequencing identifies a significant variant in methionyl-tRNA synthetase (*MARS*) in a family with late-onset CMT2. *J Neurol Neurosurg Psychiatry* 84:1247–1249. <https://doi.org/10.1136/jnnp-2013-305049>
- Hassan SA, Steinbach PJ (2011) Water-exclusion and liquid-structure forces in implicit solvation. *J Phys Chem B* 115:14668–14682. <https://doi.org/10.1021/jp208184e>
- Havrylenko S, Mirande M (2015) Aminoacyl-tRNA synthetase complexes in evolution. *Int J Mol Sci* 16:6571–6594. <https://doi.org/10.3390/ijms16036571>
- Karaca E, Harel T, Pehlivan D, Jhangiani SN, Gambin T, Coban Akdemir Z, Gonzaga-Jauregui C, Erdin S, Bayram Y, Campbell IM, Hunter JV, Atik MM, Van Esch H, Yuan B, Wiszniewski W, Isikay S, Yesil G, Yuregir OO, Tug Bozdogan S, Aslan H, Aydin H, Tos T, Aksoy A, De Vivo DC, Jain P, Geckinli BB, Sezer O, Gul D, Durmaz B, Cogulu O, Ozkinay F, Topcu V, Candan S, Cebi AH, Ikbali M, Yilmaz Gulec E, Gezdirici A, Koparir E, Ekici F, Coskun S, Cicek S, Karaer K, Koparir A, Duz MB, Kirat E, Fenercioglu E, Ulucan H, Seven M, Guran T, Elcioglu N, Yildirim MS, Aktas D, Alikasifoglu M, Ture M, Yakut T, Overton JD, Yuksel A, Ozen M, Muzny DM, Adams DR, Boerwinkle E, Chung WK, Gibbs RA, Lupski JR (2015) Genes that affect brain structure and function identified by rare variant analyses of mendelian

- neurologic disease. *Neuron* 88:499–513. <https://doi.org/10.1016/j.neuron.2015.09.048>
- Kopajtich R, Murayama K, Janecke AR, Haack TB, Breuer M, Knisely AS, Harting I, Ohashi T, Okazaki Y, Watanabe D, Tokuzawa Y, Kotzaeridou U, Kolker S, Sauer S, Carl M, Straub S, Entenmann A, Gizewski E, Feichtinger RG, Mayr JA, Lackner K, Strom TM, Meitinger T, Muller T, Ohtake A, Hoffmann GF, Prokisch H, Stauffer C (2016) Biallelic IARS mutations cause growth retardation with prenatal onset, intellectual disability, muscular hypotonia, and infantile hepatopathy. *Am J Hum Genet* 99:414–422. <https://doi.org/10.1016/j.ajhg.2016.05.027>
- Kraulis P (1991) MOLSCRIPT: a program to produce both detailed and schematic plots of protein structures. *J Appl Crystallogr* 24:946–950. <https://doi.org/10.1107/s0021889891004399>
- Latour P, Thauvin-Robinet C, Baudelet-Mery C, Soichot P, Cusin V, Faivre L, Locatelli MC, Mayencon M, Sarcey A, Broussolle E, Camu W, David A, Rousson R (2010) A major determinant for binding and aminoacylation of tRNA(Ala) in cytoplasmic Alanyl-tRNA synthetase is mutated in dominant axonal Charcot-Marie-Tooth disease. *Am J Hum Genet* 86:77–82. <https://doi.org/10.1016/j.ajhg.2009.12.005>
- Lo WS, Gardiner E, Xu Z, Lau CF, Wang F, Zhou JJ, Mendlein JD, Nangle LA, Chiang KP, Yang XL, Au KF, Wong WH, Guo M, Zhang M, Schimmel P (2014) Human tRNA synthetase catalytic nulls with diverse functions. *Science* 345:328–332. <https://doi.org/10.1126/science.1252943>
- Marchler-Bauer A, Bo Y, Han L, He J, Lanczycki CJ, Lu S, Chitsaz F, Derbyshire MK, Geer RC, Gonzales NR, Gwadz M, Hurwitz DI, Lu F, Marchler GH, Song JS, Thanki N, Wang Z, Yamashita RA, Zhang D, Zheng C, Geer LY, Bryant SH (2017) CDD/SPARCLE: functional classification of proteins via subfamily domain architectures. *Nucl Acid Res* 45:D200–D203. <https://doi.org/10.1093/nar/gkw1129>
- Merritt EA, Bacon DJ (1997) Raster3D: photorealistic molecular graphics. *Methods Enzymol* 277:505–524
- Musante L, Puttmann L, Kahrizi K, Garshasbi M, Hu H, Stehr H, Lipkowitz B, Otto S, Jensen LR, Tzschach A, Jamali P, Wienker T, Najmabadi H, Ropers HH, Kuss AW (2017) Mutations of the aminoacyl-tRNA-synthetases SARS and WARS2 are implicated in the aetiology of autosomal recessive intellectual disability. *Hum Mutat*. <https://doi.org/10.1002/humu.23205>
- Oprescu SN, Griffin LB, Beg AA, Antonellis A (2017) Predicting the pathogenicity of aminoacyl-tRNA synthetase mutations. *Methods* 113:139–151. <https://doi.org/10.1016/j.ymeth.2016.11.013>
- Pang YLJ, Martinis SA (2009) A paradigm shift for the amino acid editing mechanism of human cytoplasmic leucyl-tRNA synthetase. *Biochemistry* 48:8958–8964. <https://doi.org/10.1021/bi901111y>
- Singh H, Zhao M, Chen Q, Wang Y, Li Y, Kaitu'u-Lino TJ, Tong S, Nie G (2015) Human HtrA4 expression is restricted to the placenta, is significantly up-regulated in early-onset preeclampsia, and high levels of HtrA4 cause endothelial dysfunction. *J Clin Endocrinol Metab* 100:E936–E945. <https://doi.org/10.1210/jc.2014-3969>
- Stephen J, Vilboux T, Haberman Y, Pri-Chen H, Pode-Shakked B, Mazaheri S, Marek-Yagel D, Barel O, Di Segni A, Eyal E, Hout-Siloni G, Lahad A, Shalem T, Rechavi G, Malicdan MC, Weiss B, Gahl WA, Anikster Y (2016) Congenital protein losing enteropathy: an inborn error of lipid metabolism due to DGAT1 mutations. *Eur J Hum Genet* 24:1268–1273. <https://doi.org/10.1038/ejhg.2016.5>
- Stephen J, Vilboux T, Mian L, Kuptanon C, Sinclair CM, Yildirimli D, Maynard DM, Bryant J, Fischer R, Vemulapalli M, Mullikin JC, Huizing M, Gahl WA, Malicdan MC, Gunay-Aygun M (2017) Mutations in KIAA0753 cause Joubert syndrome associated with growth hormone deficiency. *Hum Genet* 136:399–408. <https://doi.org/10.1007/s00439-017-1765-z>
- Taft RJ, Vanderver A, Leventer RJ, Damiani SA, Simons C, Grimmond SM, Miller D, Schmidt J, Lockhart PJ, Pope K, Ru K, Crawford J, Rosser T, de Co IF, Juneja M, Verma IC, Prabhakar P, Blaser S, Raiman J, Pouwels PJ, Bevova MR, Abbink TE, van der Knaap MS, Wolf NI (2013) Mutations in DARS cause hypomyelination with brain stem and spinal cord involvement and leg spasticity. *Am J Hum Genet* 92:774–780. <https://doi.org/10.1016/j.ajhg.2013.04.006>
- Tamura K, Himeno H, Asahara H, Hasegawa T, Shimizu M (1991) Identity determinants of *E. Coli* tRNA-Val. *Biochem Biophys Res Commun* 177:619–623
- Tsai PC, Soong BW, Mademan I, Huang YH, Liu CR, Hsiao CT, Wu HT, Liu TT, Liu YT, Tseng YT, Lin KP, Yang UC, Chung KW, Choi BO, Nicholson GA, Kennerson ML, Chan CC, De Jonghe P, Cheng TH, Liao YC, Zuchner S, Baets J, Lee YC (2017) A recurrent WARS mutation is a novel cause of autosomal dominant distal hereditary motor neuropathy. *Brain*. <https://doi.org/10.1093/brain/awx058>
- Wolf NI, Salomons GS, Rodenburg RJ, Pouwels PJ, Schieving JH, Derks TG, Fock JM, Rump P, van Beek DM, van der Knaap MS, Waisfisz Q (2014) Mutations in RARS cause hypomyelination. *Ann Neurol* 76:134–139. <https://doi.org/10.1002/ana.24167>
- Zhang X, Ling J, Barcia G, Jing L, Wu J, Barry BJ, Mochida GH, Hill RS, Weimer JM, Stein Q, Poduri A, Partlow JN, Ville D, Dulac O, Yu TW, Lam AT, Servattalab S, Rodriguez J, Boddaert N, Munnich A, Colleaux L, Zon LI, Soll D, Walsh CA, Nabout R (2014) Mutations in QARS, encoding glutaminyl-tRNA synthetase, cause progressive microcephaly, cerebral-cerebellar atrophy, and intractable seizures. *Am J Hum Genet* 94:547–558. <https://doi.org/10.1016/j.ajhg.2014.03.003>